Acta Geotechnica
https://doi.org/10.1007/s11440-020-00987-9

RESEARCH PAPER

Monotonic behavior of interface shear between carbonate sands and steel

Shengjie Rui[1] · Lizhong Wang[1] · Zhen Guo[1] · Xiaoming Cheng[2] · Bo Wu[2]

Received: 5 November 2018 / Accepted: 11 May 2020
© Springer-Verlag GmbH Germany, part of Springer Nature 2020

Abstract
The characteristic of interface shear between carbonate sands and steel is important for the design of onshore/offshore foundations in coral reef deposit. By using an interface ring shear apparatus, the influences of particle size, normal stress, steel roughness and shear displacement on the interface shear strength were studied in this paper. During the tests, the particle movement localized in the deformation band was observed and the degree of particle breakage was evaluated. The test results showed that under the effect of large displacement interface shear ($\geq$ 1 m), a significant particle breakage occurred in the thin zone near the interface, and the roughness of steel interface decreased accordingly. The relative smooth steel surface shows small interface friction angle without dilation phenomenon during shearing, while higher roughness leads to higher interface strength due to stress dilation. It was also found that there was a kind of particle size discontinuity in the shear zone. Particle breakage is main reason for the increase in interface friction angle in large displacement shear. A new dimensionless parameter was proposed to consider the influences of particle breakage and interface roughness on the mobilization of interface strength between sands and steel. It is recommended that the influence of fine particles embedded into steel interface should be considered in large displacement shear for carbonate sands.

Keywords Carbonate sands · Interface friction angle · Large displacement shear · Particle breakage · Particle size distribution · Steel

1 Introduction

Carbonate sands are the product of various biological, physical, and chemical effects. There are significant differences in the mechanical performance between carbonate sands and quartz sands [4]. The carbonate sands will be easily broken or damaged into smaller particles under exterior loads. The main reason of this most notable feature is as follows: Firstly, particle hardness of carbonate sands is much lower than that of quartz sands [19]; secondly, carbonate sand particles are generally made of shells and corals that include cavities inside their bodies or on their surfaces [6, 16, 17, 31], so they have a large amount of intra-particle void space; thirdly, their irregular particle shapes are in various forms, such as curved flat particles or hollow tubular particles, resulting in significant intergranular space [30].

In practical engineering, the interaction between the structure surface and sands has an important influence on the installation resistance and bearing capacity of the foundation, of which the steel–sand interface strength is one of the most concerns. It is true that the interface shear behavior is influenced by many factors, e.g., normal stress, initial void ratio, steel roughness, mean particle size. Among which, the relationship between surface roughness and mean particle size is thought as an important factor to influence the interface behavior [7, 8, 12, 20, 25]. Dietz and Lings [11] divided the roughness into three zones (smooth, intermediate and rough) according to the value of R_a/D_{50} (R_a refers to a centerline average roughness indicating the height and spacing of peaks along the surface) and considered the influence of normal stress is depended on the normalized roughness (R_a/D_{50}). If the surface becomes

✉ Zhen Guo
nehzoug@163.com

[1] Key Laboratory of Offshore Geotechnics and Material of Zhejiang Province, College of Civil Engineering and Architecture, Zhejiang University, Hangzhou, China

[2] China Ship Scientific Research Center, Wuxi, China

Published online: 26 May 2020

rough, the dilation/contraction behavior will become obvious under lower normal stress rather than high normal stress [8]. Peak strength with smooth interface increases very slightly with increasing stress level [11, 20]. It has been acknowledged that the shear rate has negligible effect on the shearing behavior of sands tested in ring shear devices [28]. The thickness of shear zone (t) would affect the interface behavior and is mainly related to the mean particle size [13, 15, 34]. Frost et al. [13] recommended a curve derived from trend lines using the t/D_{50} against D_{50}. Ho et al. [15] proposed a curve described by $t = 10D_{50} - 5D_{50}^2$ up to $D_{50} = 1$ mm, and t keeps unchanged when D_{50} is larger than 1 mm. In generally, according to the magnitude of shear displacement, the interface shear between sands and steel can be divided into two categories: small and large shear displacement. The former one mainly focused on the peak interface strength and the mechanical behavior of the interface (hardening or softening phenomena) under small displacement. It had been proved that the interface strength has a good correspondence with R_a/D_{50} [7, 11, 12, 18, 20, 23–25]. The latter one focused on the soil resistance of the pile foundation during its large-displacement shearing. The characteristics, such as interface friction angle, grain gradation, shear zone, and interface roughness, have been experimentally studied in the last decades, among which ring shear apparatus was often used because of permitting unlimited shear displacements without having to stop and reverse. The ring shear apparatus was also adopted for the large strain shear of soil sample [5, 21, 27–29, 33, 35]. Based on the large-displacement interface ring shear test, Yang et al. [34] found the shear zone thicknesses and crushed fine fractions increase with normal stress and displacement. Ho et al. [15] pointed out that the particle breakage within shear zone and the change of interface roughness affected the mobilization of interface friction angle.

In previous works, the interface shear between quartz sand and steel interface has been investigated, but research works about carbonate sand are very limited. In order to reveal the mechanism of the interface shear between the carbonate sands and steel, an interface ring shear apparatus was used to study the influences of particle size, normal stress and shear displacement on the interface shear strength. The degree of particle breakage during large-displacement interface shear was evaluated, and then its effect on the mobilization of interface friction angle was discussed. The change of interface roughness and its effect were also assessed. As a comparison, the interface shear tests between quartz sands and steel were performed.

2 Design of interface shear tests

2.1 Interface materials

2.1.1 Sand samples

Two types of sand were used in the experiments: carbonate sand and quartz sand, as shown in Fig. 1. The carbonate sand was taken from the coast of an island in the South China Sea. Through XRD chemical analysis, the calcium carbonate content of these sands was known to be 98.1%. The sand specific gravity was 2.81. The used quartz sand was Pingtan standard sands in China, and its specific gravity was 2.65.

Before the experiments, the sand samples were soaked and cleaned with pure water to remove the salt on the sand surface and then placed in the oven for drying. The sands were sieved and selected into two groups of 0.1–0.25 mm and 0.5–1 mm. The mean particle sizes (D_{50}) of 0.1–0.25 mm and 0.5–1 mm are 0.175 mm and 0.75 mm, respectively. In the following sections, symbols C or Q in front of the particle size represents the groups of carbonate and quartz sands, respectively. The information about void ratios is listed in Table 1.

2.1.2 Steel interface

The steel interface used in the experiments was 1045 in the US standard [2], as shown in Fig. 2a. The tensile strength of the steel was approximately 600 MPa, and the elastic modulus was 210 GPa. Air abrading was used to control the surface roughness of the steel interface before each test. Surface roughness was measured at six different locations for each interface by a surface roughness tester (TR200, Huayi Hi-Tech Company, China), sampling over 15 mm lengths that were approximately parallel to the direction of shearing. Average roughness R_a was determined from the digitally stored outputs. The interface roughness (R_a) before interface shear was about 3.25 μm (two tests with

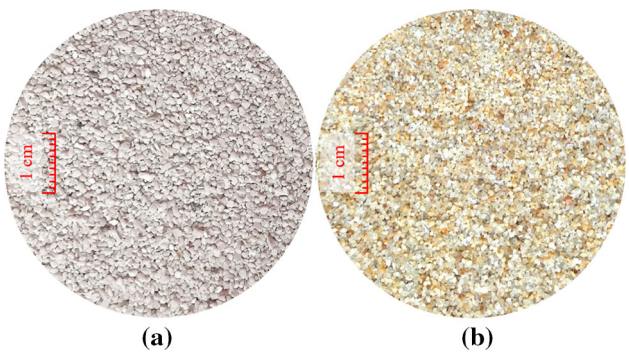

Fig. 1 Sand samples used in the experiments: **a** carbonate sand; **b** quartz sand

Table 1 Void ratios of the sand samples

Sand sample	Maximum void ratio e_{max}	Minimum void ratio e_{min}	Initial void ratio
C0.1-0.25	1.210	0.948	1.021
C0.5-1	1.321	0.970	1.068
Q0.1-0.25	0.949	0.650	0.734
Q0.5-1	0.836	0.600	0.666

R_a= 5.25 μm), and the typical profile of the interface is shown in Fig. 2b. The ratio of R_a/D_{50} corresponding to 0.1–0.25 mm sand and 0.5–0.1 mm sand are 0.0186 and 0.0043 with R_a= 3.25 μm, 0.0300 and 0.0069 with R_a= 5.25 μm, which both belong to the intermediate rough range according to research work by Dietz and Lings [11].

2.2 Experimental apparatus

As shown in Fig. 3, the interface ring shear apparatus mainly includes the shear ring, force transmission rod, control motor, air cylinder, force sensor, torque sensor, angle sensor, and other elements. The diameters of the outer and inner ring are 300 mm and 200 mm, respectively. The ratio of outer to inner ring diameter is 1.5. Bishop et al. [3] recommended the same ratio for ring shear apparatus. The configuration of interface ring shear apparatus is shown in Fig. 4. In this work, the lower interface configuration was adopted, i.e., the sands were in the upper ring and the steel interface was equipped in the lower ring.

The interface strength in this paper refers to the mobilized interface friction angle δ_{cs} under constant normal stress σ_{cs}, meaning that this kind of test belongs to constant

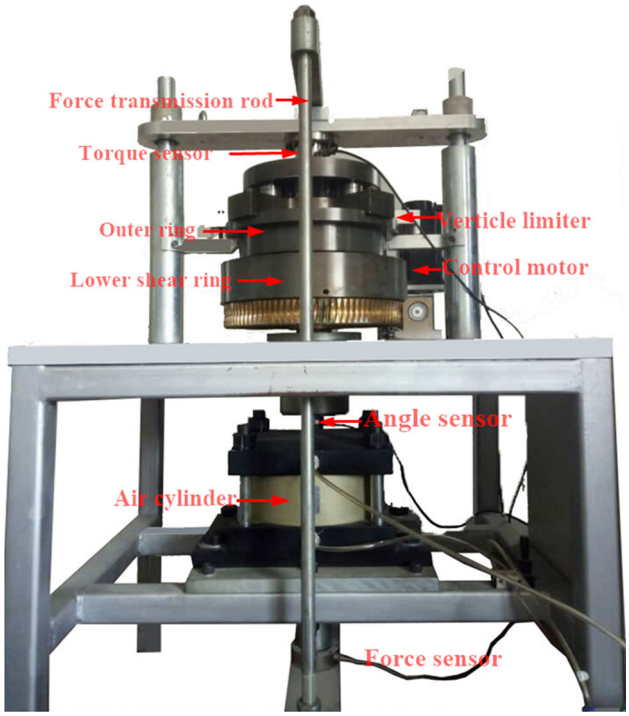

Fig. 3 Interface ring shear apparatus

normal load (CNL) condition. The interface behavior also strongly depends on boundary conditions of the entire system (expressed by, e.g., the different specimen size, initial stress state, initial void ratio distribution, confining condition). It means that the sand behavior during interface shear in a ring shear apparatus is, in general, different from that at piles. The normal force exerted on the interface is denoted by W. The shear stress on the interface is τ and the measured torque is M. The radiuses of the outer and inner rings are R_2 and R_1, respectively. Thus, the interface friction angle δ_{cs} can be calculated by

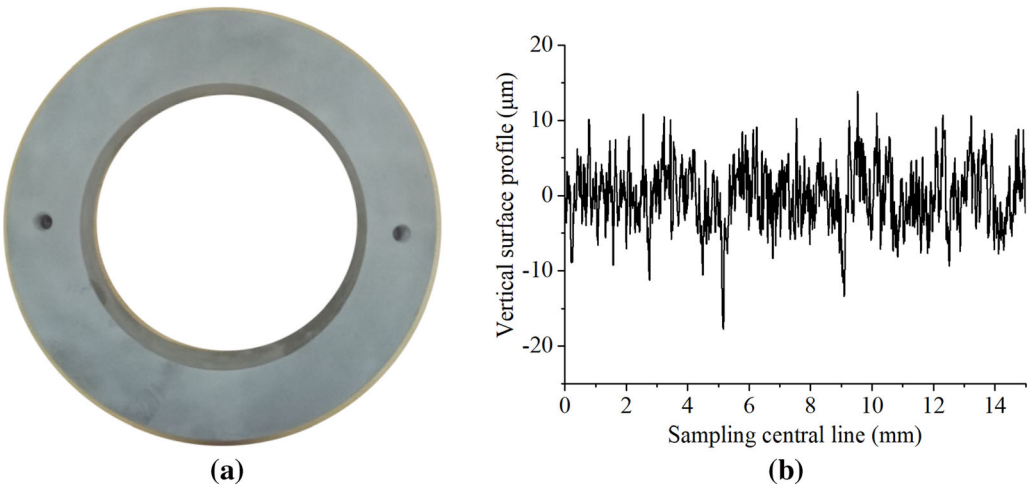

Fig. 2 Steel interface and typical interface profile: **a** steel interface; **b** typical interface profile

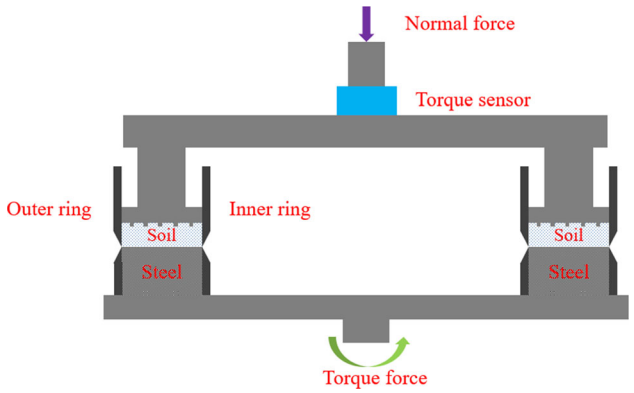

Fig. 4 Configuration of interface ring shear apparatus

$$\sigma_{cs} = \frac{W}{\pi(R_2^2 - R_1^2)} \tag{1}$$

$$\tau = \frac{3M}{2\pi(R_2^3 - R_1^3)} \tag{2}$$

$$\delta_{cs} = \tan^{-1}\left(\frac{\tau}{\sigma_{cs}}\right) \tag{3}$$

2.3 Test design and procedures

Before the test, air-abrading was performed to control the roughness of the steel interface to reach the test requirements. The sand samples were prepared with air pluviation. Dry sands were poured into a funnel with a falling height of 10 cm. The final height of sand sample was 20 mm, and the relative density was about 72%. Shear displacement was exerted after the sample preparation was completed. The interface friction angle was continuously measured in the first 50 mm shear displacement. In order to reduce sand leakage, the gap between upper and lower rings was closed using the vertical limiter in the subsequent large-displacement shear process. The gap between the upper and lower rings was reopened only at the specific 0.5 m, 1 m, and 2 m shear displacement to measure the mobilized δ_{cs}. In order to minimize the disturbance due to opening the gap, three measures were used in the tests. Firstly, the silicon grease was applied on the confining wall before tests to reduce the wall friction. Secondly, the maximum opening gap was set to be only 0.3 mm to reduce the disturbance [5, 34]. Thirdly, the height of soil sample was 20 mm, which was relative thin compared to the soil width 50 mm. So, the influence of wall friction on the interface normal stress could be decreased to a lower level. After each test, the thickness of shear zone, the particle size and the interface roughness were measured, and the shape of broken particles was observed by a scanning electron microscope.

Table 2 shows the design of all the interface ring shear tests. The normal stress applied on the interface was equal to 50 kPa, 100 kPa, 200 kPa, and 300 kPa. Sadrekarimi and Olson [28] considered the shear rate had negligible effect on sands test in ring shear devices. Yang et al. [34] and Ho et al. [15] used a wide range shear speed from 0.9 to 250 mm/min. The shear rate in the test was set to be 5.45 mm/min. 34 groups of tests were carried out in monotonic shear. Test M1 to M16 aimed to investigate the effect of the normal stress on the mobilized interface friction angle, while the test M17 to M30 focused on the effect of shear displacement. Two tests (M31, M32) with higher interface roughness were conducted for comparison. In addition, four groups using the transparent outer ring were performed to observe the formation and development of concentrated deformation band near the interface.

3 Test results and interpretation

3.1 Interface friction angle

Figure 5a, b shows the mobilized interface friction angles δ_{cs} between carbonate sands and steel versus shear displacement. δ_{cs} values reach a peak within 5 mm shear displacement, and then decrease gradually. But, after 0.5 m shear displacement, δ_{cs} values show an increase trend again. It is found that δ_{cs} values for carbonate sands have certain normal stress dependence. In addition, with the increase in the normal stress, the interface friction angle δ_{cs} for coarser sands (C0.5-1) increases more obvious than the fine carbonate sands (C0.1-0.25). The reason for this stress-dependent behavior may be that under a greater normal stress, the stress concentration on the protrusion of carbonate sands causes the particle breaking up, resulting in a stronger interlock with the steel interface. DeJong et al. [9, 10], DeJong and Westgate [8] studied the steel–sand interface shear behavior and pointed out that the particle angularity would lead to higher interface strength under CNL condition. Our work is consistent with the research from DeJong et al. [9, 10] and DeJong and Westgate [8].

Figure 5c, d shows the variations of interface friction angle δ_{cs} for two quartz sands versus shear displacement. The friction angle δ_{cs} between Q0.5-1 sand and steel increases with shear displacement, and becomes stable after 2 m shear displacement. The peak strength of Q0.5-1 sand is not observed in the test. The mobilized strength of Q0.5-1 sand shows a continuous increasing trend. This is because R_a/D_{50} of the sand in the beginning is relatively low (according to Sect. 2.1) and the surfaces of quartz sand are relatively smooth (according to Sect. 4.1). Compared to the Q0.5-1 sand, the interface friction angle δ_{cs} for Q0.1-0.25 sand decreases after the peak, and then

Table 2 Design of interface ring shear tests

Test code	Sand sample	Normal stress (kPa)	R_a (μm)	Shear displacement (m)
M1	C0.5-1 sand	50	3.25	2
M2	C0.5-1 sand	100	3.25	2
M3	C0.5-1 sand	200	3.25	2
M4	C0.5-1 sand	300	3.25	2
M5	C0.1-0.25 sand	50	3.25	2
M6	C0.1-0.25 sand	100	3.25	2
M7	C0.1-0.25 sand	200	3.25	2
M8	C0.1-0.25 sand	300	3.25	2
M9	Q0.5-1 sand	50	3.25	2
M10	Q0.5-1 sand	100	3.25	2
M11	Q0.5-1 sand	200	3.25	2
M12	Q0.5-1 sand	300	3.25	2
M13	Q0.1-0.25 sand	50	3.25	2
M14	Q0.1-0.25 sand	100	3.25	2
M15	Q0.1-0.25 sand	200	3.25	2
M16	Q0.1-0.25 sand	300	3.25	2
M17	C0.5-1 sand	100	3.25	0.5
M18	C0.5-1 sand	100	3.25	1
M19	C0.5-1 sand	100	3.25	4
M20	C0.5-1 sand	100	3.25	8
M21	C0.1-0.25 sand	100	3.25	0.5
M22	C0.1-0.25 sand	100	3.25	1
M23	C0.1-0.25 sand	100	3.25	4
M24	C0.1-0.25 sand	100	3.25	8
M25	Q0.5-1 sand	100	3.25	1
M26	Q0.5-1 sand	100	3.25	4
M27	Q0.5-1 sand	100	3.25	8
M28	Q0.1-0.25 sand	100	3.25	1
M29	Q0.1-0.25 sand	100	3.25	4
M30	Q0.1-0.25 sand	100	3.25	8
M31	C0.5-1 sand	50	5.25	2
M32	C0.5-1 sand	100	5.25	2
M33	C0.5-1 sand	200	5.25	2
M34	C0.5-1 sand	300	5.25	2
M35	C0.1-0.25 sand	50	5.25	2
M36	C0.1-0.25 sand	100	5.25	2
M37	C0.1-0.25 sand	200	5.25	2
M38	C0.1-0.25 sand	300	5.25	2
M39*	C0.5-1 sand	100	5.25	2
M40*	C0.1-0.25 sand	100	5.25	2
M41*	C0.5-1 sand	100	3.25	0.5
M42*	C0.1-0.25 sand	100	3.25	0.5
M43*	Q0.5-1 sand	100	3.25	0.5
M44*	Q0.1-0.25 sand	100	3.25	0.5

The superscript * is corresponding to the interface shear tests using transparent outer ring

increases until reaching a stable value. The interface friction angle variation for Q0.1-0.25 sand is similar to that of the carbonate sands. However, the two quartz sands do not show normal stress dependence. It is also found that δ_{cs} value for Q0.1-0.25 sand is bigger than that for Q0.5-1 sand in small shear displacement, e.g., the fine sands generally show higher peak interface strength than the coarse sands. This is because the fine sands are more easily embedded in the interface with the same interface roughness, thus mobilizing bigger interface friction angle δ_{cs} [22].

Figure 6 shows typical vertical displacement against shear displacement under 100 kPa for quartz and carbonate sands. It is shown that the main trend of these two sands after large-displacement interface shear is the volume contraction. The C0.5-1 sand has maximum volume contraction, followed by the Q0.5-1 sand. Fine sands (C0.1-0.25 and Q0.1-0.25) show less volume contraction compared to the coarse sands (C0.5-1 and Q0.5-1). For small displacement shear shown in Fig. 6b, the interface shear of fine sands shows slight dilation trend, while the dilation phenomena with coarse sands are not apparent mainly because of the relative smooth interface (R_a/D_{50}). With the increase in shear displacement, the particle breakage becomes the main reason for volume contraction.

Figure 7 presents the interface shear results for two steel surface roughness (R_a= 3.25 μm and 5.25 μm) under 100 kPa. Figure 7a indicates that interface with R_a= 5.25 μm mobilizes higher strength compared to that with the relative smooth interface (R_a= 3.25 μm). After large-displacement shear, the roughness still contributes to exert higher interface strength. For a smaller shear displacement, C0.1-0.25 sand mobilizes higher interface strength than C0.5-1 sand mainly because of higher normalized roughness (R_a/D_{50}). Figure 7b shows the vertical displacement against shear displacement. These sands all show contraction trend initially. The dilation with relative smooth interface (R_a= 3.25 μm) is not apparent, while interface with R_a= 5.25 μm shows the dilation trend after 0.5 mm shear displacement, which is the reason for mobilizing higher interface strength.

3.2 Deformation band and shear zone in the sand samples

Deformation band in this paper refers to the zone that is often characterized by spontaneous localization of nonuniform deformations [1, 26, 32]. In addition, the shear zone is defined as a zone near the interface that contains a large number of obviously broken sand particles, clearly differentiated from the fresh sand particles by its special color [15]. In this section, the development of deformation band and shear zone characteristics will be presented and discussed.

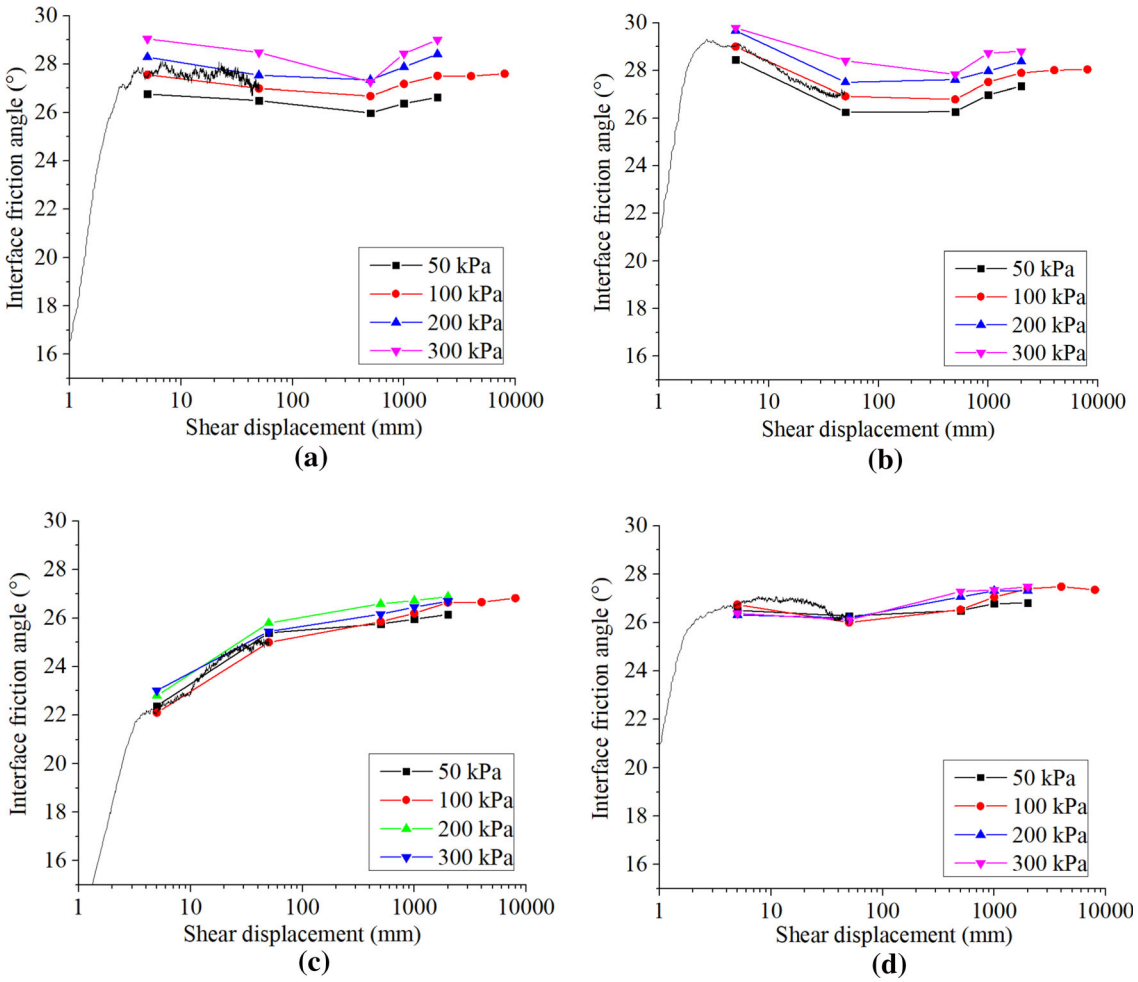

Fig. 5 Mobilized interface friction angles between different sand samples and steel versus shear displacement with R_a= 3.25 μm: **a** C0.5-1 sand; **b** C0.1-0.25 sand; **c** Q0.5-1 sand; **d** Q0.1-0.25 sand

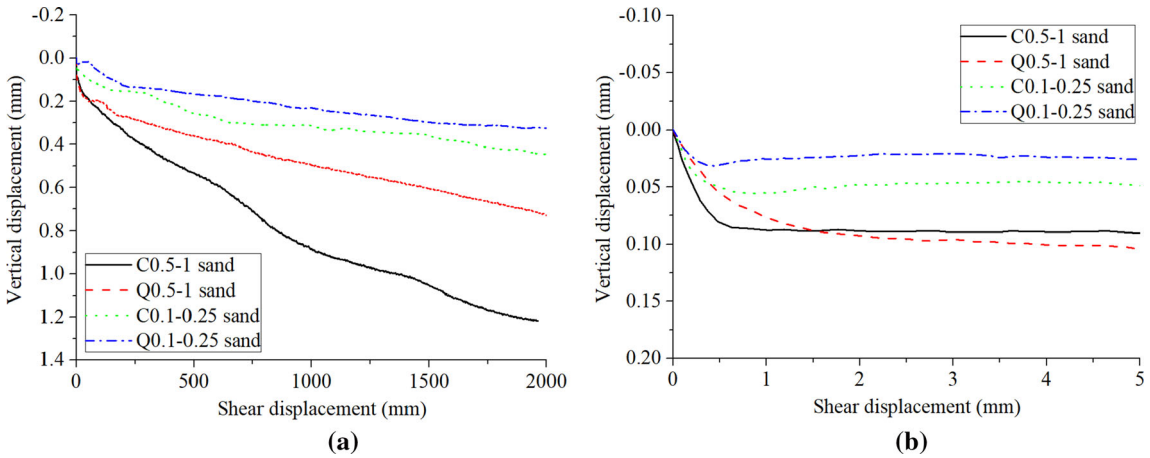

Fig. 6 Vertical displacement against shear displacement under 100 kPa with R_a= 3.25 μm: **a** shear displacement scale: 0-2 m; **b** shear displacement scale: 0-5 mm

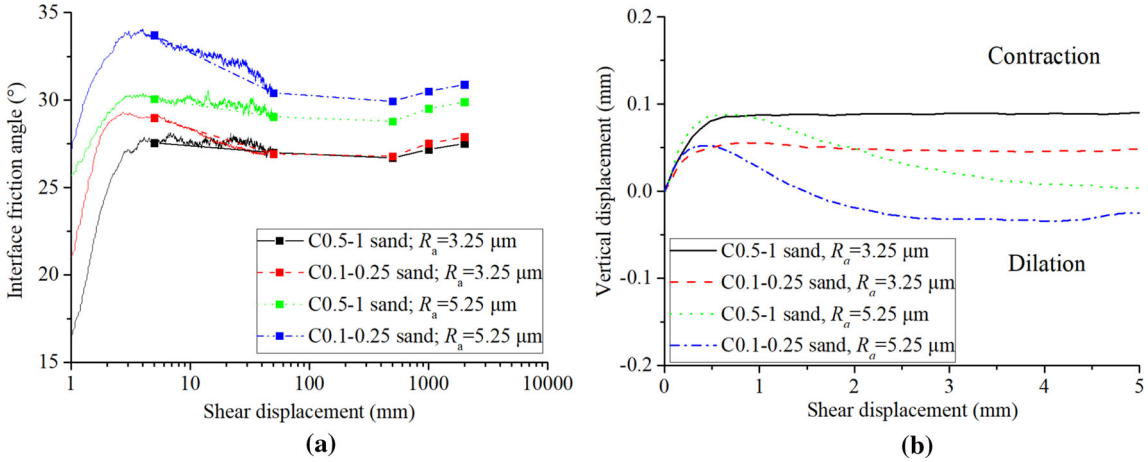

Fig. 7 Comparison with higher steel roughness (R_a= 5.25 μm) under 100 kPa: **a** interface friction angle; **b** vertical displacement

3.2.1 Deformation band of sand samples

In M31 to M34 tests, the plexiglass transparent ring was used as the outer ring to observe the deformation band formation and development [27, 29, 32]. Sand particles were colored in red ink, and then the development of the deformation band was quantitatively evaluated by the deformation of colored sands. Figure 8 presents a series of photos about the development of deformation band with shear displacement s with R_a= 3.25 μm. It is shown that the sand sample deformation can be divided into two stages: uniform shear deformation stage and deformation band development stage. For coarse sands (C0.5-1 and Q0.5-1), when the shear displacement is applied at the beginning, uniform shear deformation of the sand sample appears in the vertical direction of 20 mm height. The interface friction angle δ_{cs} reaches its peak at the end of this stage. C0.5-1 sand needs 3.0 mm while Q0.5-1 sand needs 3.6 mm to reach the peak. In the following stage, the shear localization occurs near the interface, i.e., the deformation band starts to form and develop. The sand particles near the interface move simultaneously along with the interface, and the main movement pattern is rolling between particles.

The development trend of deformation band for fine sands (C0.1-0.25 and Q0.1-0.25) is roughly consistent with that for coarse sands. The differences are as follows: for fine sands, only the sand particles near the interface have a uniform deformation with a thickness of about 6–8 mm; secondly, two fine sands need smaller shear displacement to reach its peak interface strength (2.6 mm for C0.1-0.25 sand, 2.5 mm for Q0.1-0.25 sand); thirdly, the deformation band thicknesses for fine sands is apparently smaller than that for coarse sands.

Figure 9 presents deformation band of the carbonate sand with higher roughness R_a = 5.25 μm. The deformation band also has two stages: uniform shear deformation stage and deformation band development stage. With higher surface roughness, C0.5-1 sand needs 3.2 mm while C0.1-0.25 sand needs 2.8 mm to reach the peak δ_{cs} at the end of uniform shear deformation stage, and the displacement is a little higher than that of R_a = 3.25 μm (3.0 mm and 2.6 mm, respectively). In the deformation band development stage, the deformation band thickness with R_a = 5.25 μm is apparent higher than that of R_a = 3.25 μm, indicating that more particles move along with the steel surface with higher roughness.

Figure 10 shows the displacement profiles for four sand samples at different shear displacements with R_a= 3.25 μm. The profiles were obtained from the left boundary of the colored sand particles. As to C0.5-1 and Q0.5-1 sands, the particles within 3.5 mm height ($5D_{50}$) move with the interface. The displacement of sand particles closest to the interface is lagged behind the interface displacement, indicating some degree of relative displacement between sands and interface. In addition, the displacement of C0.5-1 sand is larger than that of Q0.5-1 sand, and the vertical direction displacement attenuates more slowly. In contrast, the thickness of moving particles for fine sands (C0.1-0.25 and Q0.1-0.25 sand) is relatively small, and so is the relative displacement with the interface. Figure 11 shows comparison of displacement profiles of sand samples with R_a= 5.25 μm. With higher steel roughness, for C0.5-1 sand, the particles within 5.3 mm height (about $7.5D_{50}$) move with the interface, and relative displacement between sands and interface is smaller than that of R_a = 3.25 μm, which indicates more intense interaction with higher roughness. As to the C0.1-0.25 sand, the deformation band

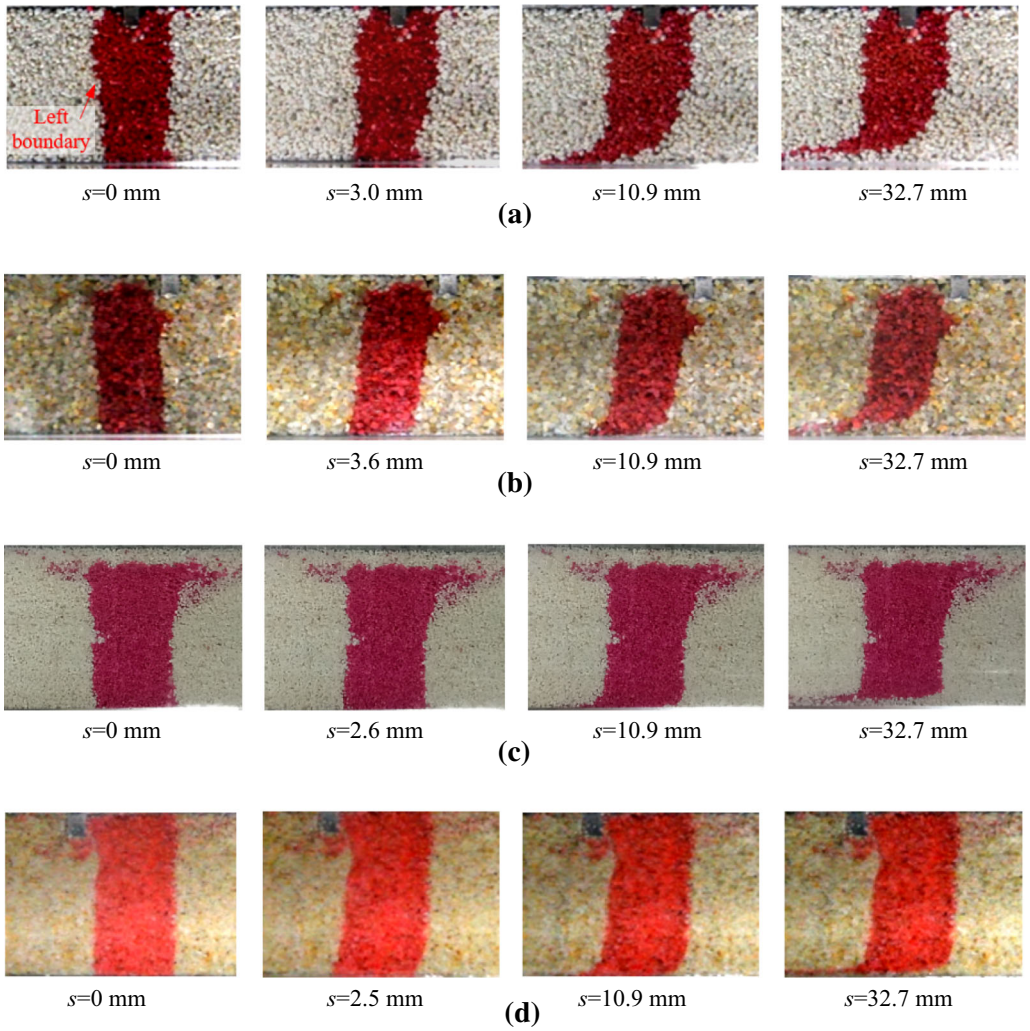

Fig. 8 Development of shear band with shear displacement with R_a= 3.25 μm: **a** C0.5-1 sand; **b** C0.1-25 sand; **c** Q0.5-1 sand; **d** Q0.1-0.25 sand

thickness can reach 3.3 mm (about $22D_{50}$), compared with 1.7 mm ($10D_{50}$) of R_a = 3.25 μm.

3.2.2 Shear zone of sand samples

The shear zone generally develops and tends to become stable with the increase in shear displacement. Figure 12 presents the photos of shear zones formed by different sand samples after 2 m displacement shear. The shear zone for quartz sands is gray, while the shear zone for carbonate sands is shown in white. The gray quartz sand is thought to contain some fine steel particles abraded from the surface [34] as the roughness of steel interface has been changed after interface shear in Sect. 3.4. The main influence is decreasing the steel roughness and increasing the fine content to some extent in the shear zone. It is found that the shear zone for coarse sands is always thicker than that for fine sands.

Figure 13 shows thickness of shear zone versus normal stress after 2 m displacement shear with R_a = 3.25 μm. It is shown that the shear zone can be more easily formed under higher normal stress. Due to the lower particle hardness, the thickness of shear zone for carbonate sands is obviously bigger than that of quartz sands. In this paper, the dimensionless parameter t/D_{50} (ratio of shear zone thickness to median particle size) is used to assess the thickness of shear zone. After 2 m displacement shear with higher roughness R_a = 3.25 μm, t/D_{50} for the fine sands is up to 8–12, while t/D_{50} for the coarse sands only reaches 3–5. Figure 14 presents comparison of shear zone thickness versus normal stress with R_a= 5.25 μm. Shear zone thickness with R_a = 5.25 μm is higher than that of R_a = 3.25 μm, especially for the CS0.5-1 sand under lower normal stress. And the t/D_{50} with higher roughness also shows higher value compared with that of R_a = 3.25 μm.

As shown in Fig. 15, the shear zone thickness t increases with the shear displacement under the normal stress

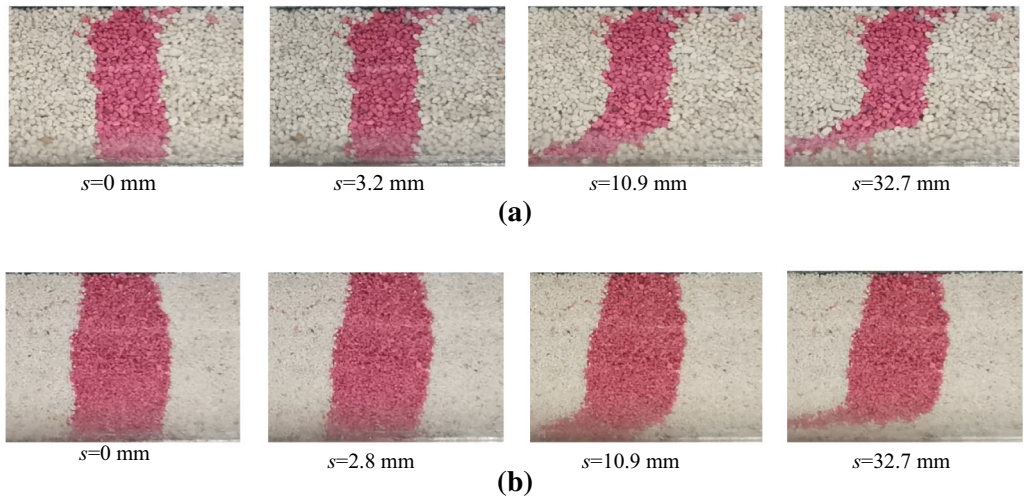

Fig. 9 Development of shear band with shear displacement with R_a= 5.25 μm: **a** C0.5-1 sand; **b** C0.1-25 sand

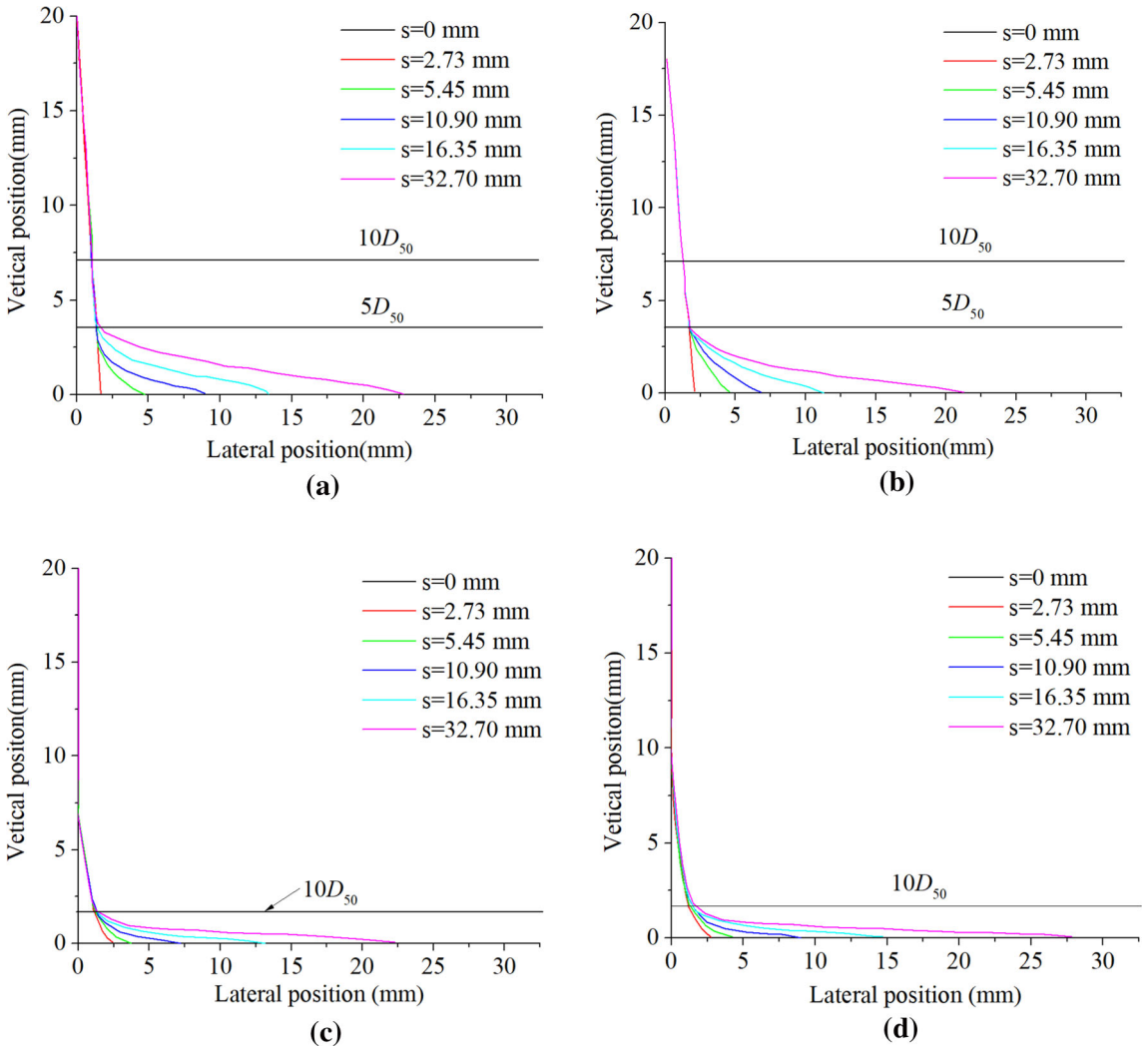

Fig. 10 Displacement profiles of sand samples at different shear displacements with R_a= 3.25 μm: **a** C0.5-1 sand; **b** C0.1-25 sand; **c** Q0.5-1 sand; **d** Q0.1-0.25 sand

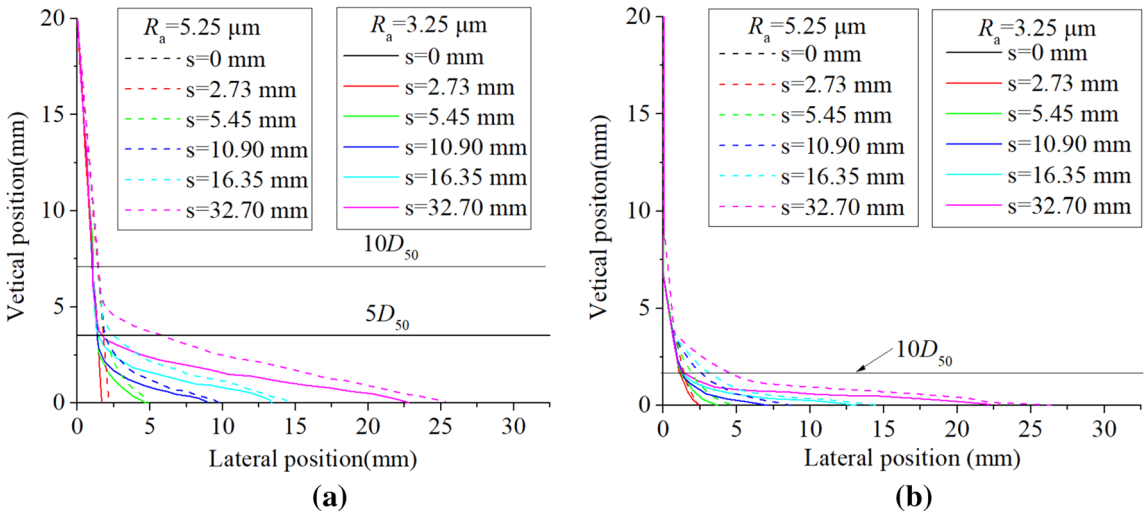

Fig. 11 Comparison of displacement profiles of sand samples with R_a= 5.25 μm: **a** C0.5-1 sand; **b** C0.1-25 sand

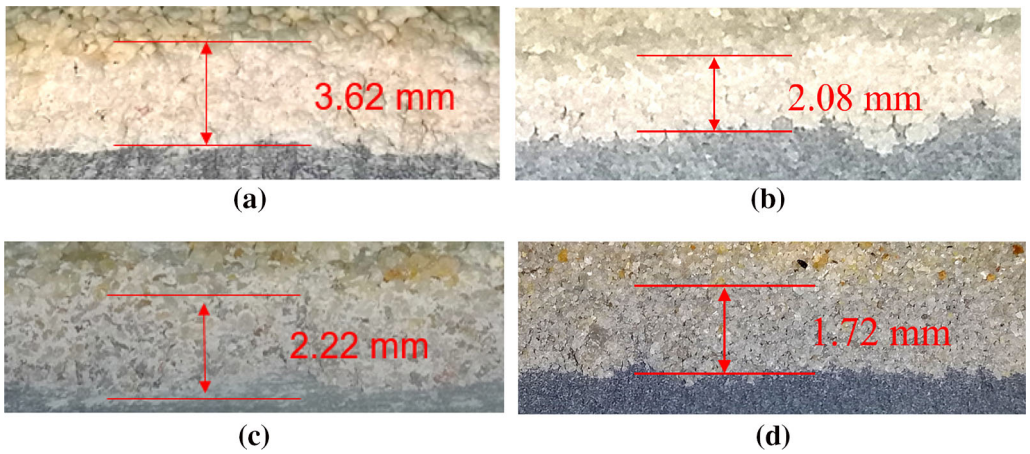

Fig. 12 Photos of shear zones for different sand samples after 2 m displacement shear: **a** C0.5-1 sand, 200 kPa; **b** C0.1-0.25 sand, 200 kPa; **c** Q0.5-1 sand, 200 kPa; **f** Q0.1-0.25 sand, 200 kPa

100 kPa. For fine sands, the thickness t develops rapidly in the first 2 m displacement and gradually stabilizes after 4 m displacement. But, for coarse sands, the shear zone thickness t increases even at 8 m shear displacement. Generally, sand samples with small particle size leads to larger t/D_{50}, i.e., t/D_{50} = 12 for fine sands and t/D_{50} = 5 for coarse sands at 8 m shear displacement.

3.2.3 Relationship between deformation band and shear zone

Comparing the deformation band and the shear zone formed under 100 kPa, it can be concluded that shear zone is formed after sand particles in the deformation band are fully broken. The thickness of the shear zone is lower at small shear displacement because of the incomplete breakage of sand particles. When the shear displacement is large enough, the particles in the deformation band are fully broken and the shear zone thickness increases gradually and tends to become equal to the deformation band thickness.

3.3 Particle size distribution and particle breakage

3.3.1 Particle size distribution

Laser particle size analyzer was used to obtain the particle size distribution (PSD) in interface shear experiments. Under different normal stresses, particle size distributions after 2 m shear displacement with R_a= 5.25 μm become different, as shown in Fig. 16. In the PSD curves, a kind of

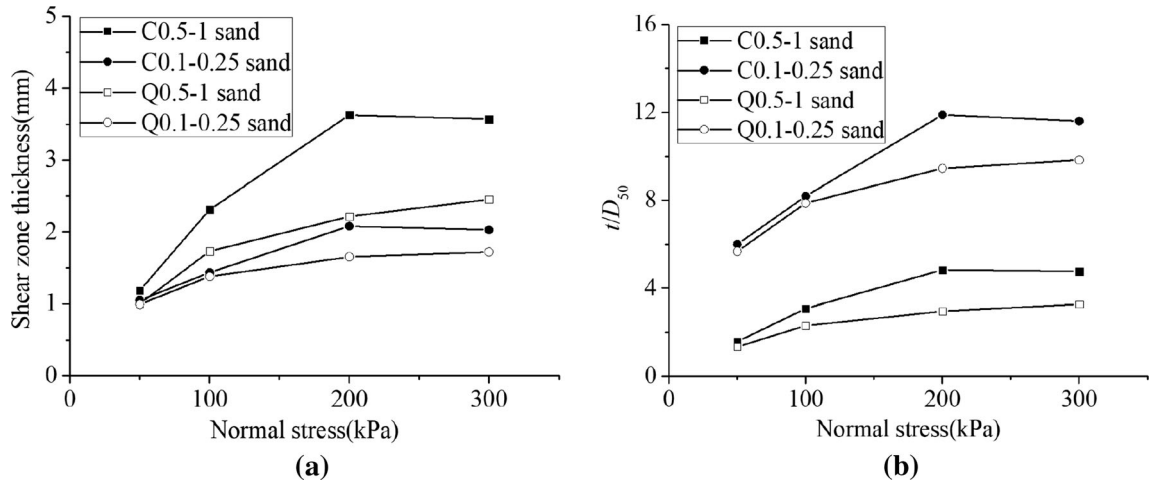

Fig. 13 Thickness of shear zone versus normal stress with R_a= 3.25 μm: **a** t compared with quartz sands; **b** t/D_{50} with quartz sands

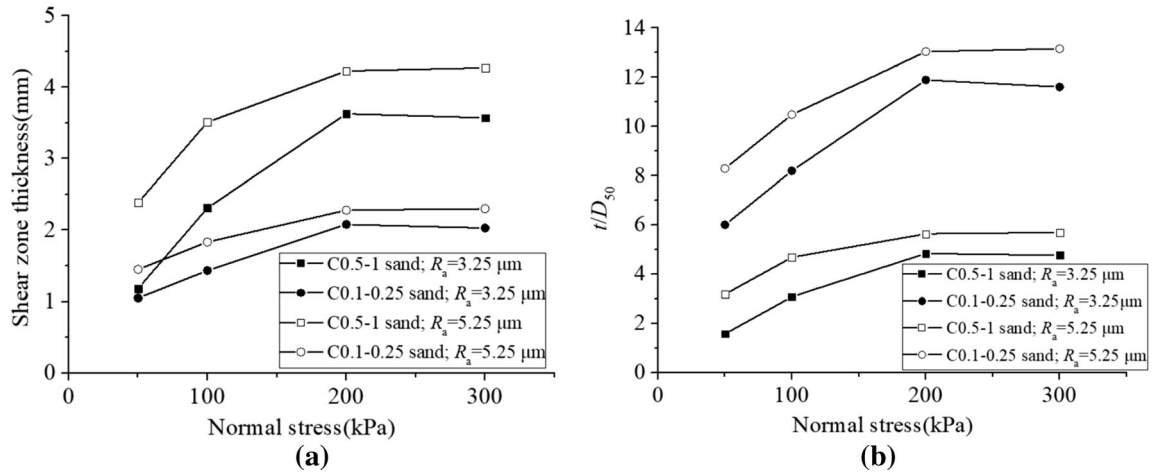

Fig. 14 Comparison of shear zone thickness versus normal stress with R_a= 5.25 μm: **a** t; **b** t/D_{50}

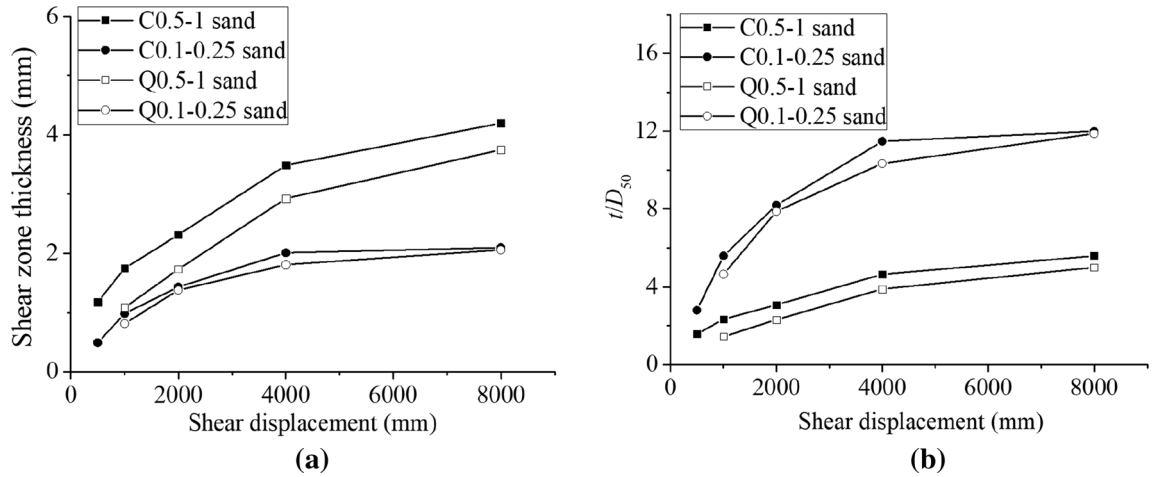

Fig. 15 Thickness of shear zone versus shear displacement under normal stress of 100 kPa: **a** shear zone thickness with shear displacement; **b** t/D_{50} with shear displacement

"grain blank segment" appears, indicating that there exists particle size discontinuity in the sand sample after interface shear. For the cases with same shear displacement, larger normal stress leads to the increase in fine particle content in the shear zone. The minimum particle size for carbonate sands is only about 0.4 μm, which is less than 2 μm for quartz sands. The shape of PSDs of fine particles formed in shear zone is like a triangle in the semi-logarithmic coordinate. Figure 17 presents comparison of PSD under different normal stresses with R_a= 5.25 μm. For C0.5-1 sand, higher steel roughness (R_a = 5.25 μm) leads to more obvious particle breakage, but it has limit influence on the particle breakage of fine sand (C0.1-0.25 sand).

Figure 18 shows PSDs for different sand samples under shear displacement with R_a= 3.25 μm. In general, with the increase in shear displacement, fine particle fraction increases gradually. The gradation curves of fine sands (C0.1-0.25 and Q0.1-0.25) at 4 and 8 m shear displacements coincide well, indicating that little particle breakage occurs after 4 m displacement shear. But for Q0.5-1 sand, particle breakage increases continuously with the increase in shear displacement, even after 8 m displacement shear. To illustrate the effect of interface shear on the PSD, Fig. 19 gives the relationship between the PSD for C0.1-0.25 sand and shear displacement under the normal stress of 100 kPa. It was suggested by Coop et al. [5] that for the case of sand–sand shear, the sand particles tend to reach a stable PSD with the increase in shear displacement, which is a straight line in double logarithmic coordinates in Fig. 19. Compared with the stable PSD after sand–sand shear, the degree of particle breakage after interface shear is lower, and particle size discontinuity will appear in the sand sample in large-displacement interface shear.

3.3.2 Particle relative breakage

Hardin [14] proposed the assessment method of relative breakage with the assumption that the particles less than 0.075 mm do not break. This assumption is not appropriate for the interface shear because a large number of fine particles (< 0.075 mm) will form. Based on the Hardin assessment method, Sadrekarimi and Olson [27, 29] extended the minimum breakage particle size to 0.001 mm to consider the effect of fine particles. Therefore, the Sadrekarimi's method is used in the calculation of the relative breakage in this paper.

Figure 20 presents the relationship between the relative breakage B_r and normal stress at 2 m shear displacement. The relative breakage of sands increases with the increase in normal stress. Compared with quartz sands, the particle breakage of carbonate sands is bigger during the process of interface shear, especially for the coarse sands. It also shows that higher roughness (R_a = 5.25 μm) increases relative breakage of C0.5-1 sand, but the B_r value remains almost the same for C0.1-0.25 sand with higher roughness.

As shown in Fig. 21, the particle relative breakage B_r increases with the increase in shear displacement under 100 kPa normal stress with R_a= 3.25 μm. For the carbonate sands, particle breakage mainly occurs within the first 2 m shear displacement, while for the quartz sands, significant breakage occurs within the shear displacement of 4 m. The particle relative breakage becomes stabilized after 4 m displacement shear, except for Q0.5-1 sand.

3.4 Steel interface roughness

In fact, accompanied by obvious breakage of sand particles, the steel interface will also be abraded after large-displacement interface shear. Figure 22a presents the photo of the steel interface after air-abrading treatment. As a comparison, Fig. 22b shows the steel interface in test M4 (C0.5-1 sand under 300 kPa after 2 m displacement shear). It can be seen that some white fine particles formed by crushed carbonate sands are embedded into the steel interface. Transforming the photo into binary image in Fig. 22c, the area occupation ratio of white fine particle is about 31.3%. The embedded fine particles make the interface shear partly (31.3% of total area) turned into the friction between sand particles. However, the interface surface was not found to be fully filled with the fine particles in the test because there is a limitation for carbonate sand to be damaged into fine particles and embedded into the interface. This phenomenon only appears in the case of large-displacement interface shear for carbonate sands. As shown in Fig. 22d, there is few fine quartz sand particles embedded into the interface after interface shear.

Figure 23a, b shows the relationships of interface roughness, normal stress and shear displacement. It is obvious in Fig. 23a that greater normal stress causes more reduction of the interface roughness, because the increase in the stress level enhances the interaction between the interface and sand particles. The coarse sands are more likely to reduce the roughness of the steel interface due to that interaction between coarse sands and interface results in severer friction between particles and interface protruding parts. As shown in Fig. 23b, the interface roughness decreases with the increase in shear displacement. For carbonate sands, the roughness reduction occurs mainly in first 2 m displacement, and tends to be stable after 4 m. While for quartz sands, the roughness reduces obviously in first 4 m, but still decreases even at 8 m. This difference may be due to: on one hand, the sands with high mineral hardness tend to change the interface more easily; on the other hand, the broken particles in shear zone are gradually embedded into the interface and thus have a protective effect on the interface. This protective effect can be

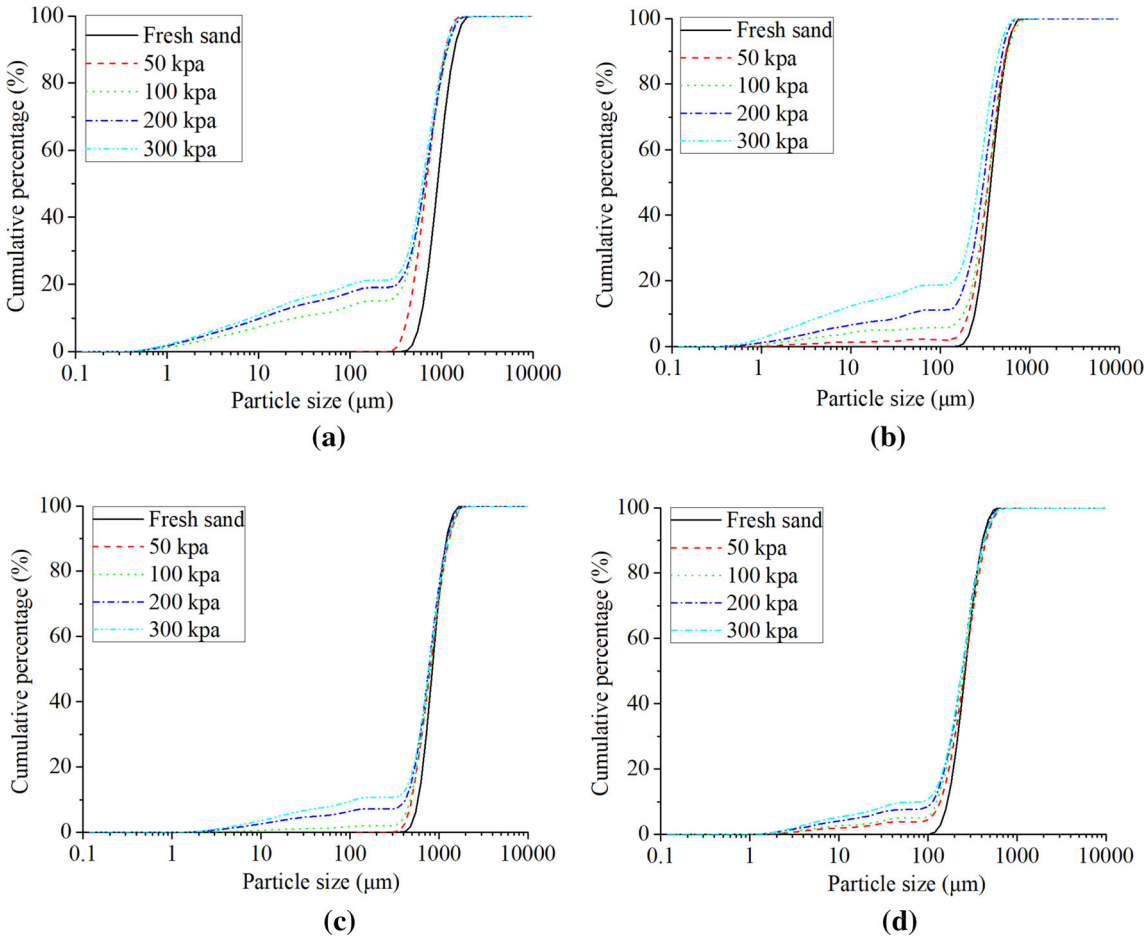

Fig. 16 Particle size distributions under different normal stresses at 2 m shear displacement with R_a= 3.25 μm: **a** C0.5-1 sand; **b** C0.1-0.25 sand; **c** Q0.5-1 sand; **d** Q0.1-0.25 sand

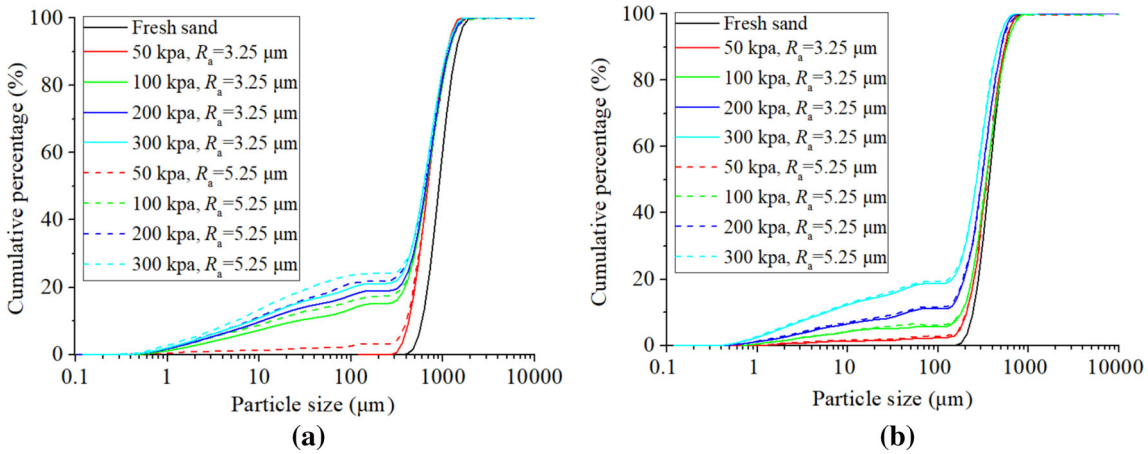

Fig. 17 Comparison of PSD under different normal stresses with R_a= 5.25 μm: **a** C0.5-1 sand; **b** C0.1-0.25 sand

explained as follows: For carbonate sand, some fine particles are gradually embedded into the steel surface. This leads to a kind of sand–sand shearing in the embedment area. So, the steel surface can be protected and its roughness keeps almost unchanged after 4 m shear displacement during the tests.

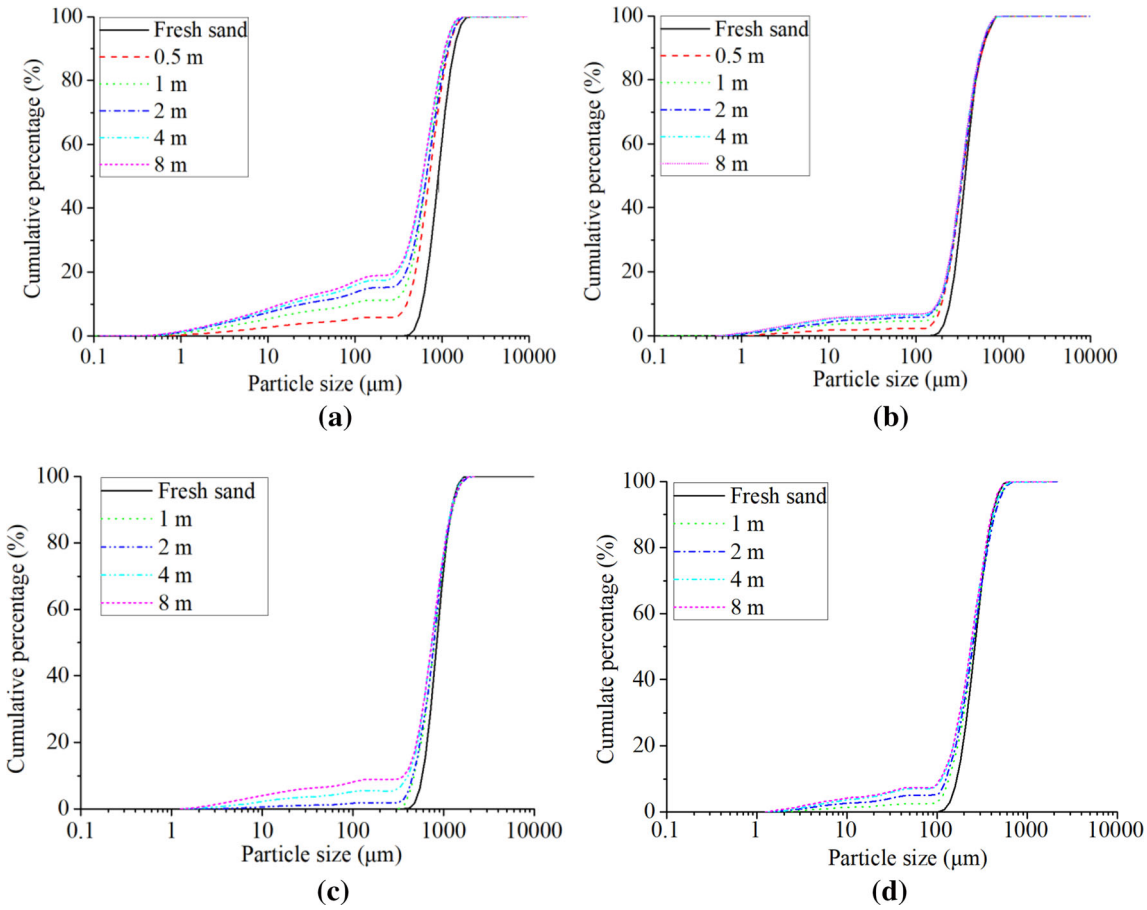

Fig. 18 PSDs for different sand samples under shear displacement with R_a= 3.25 μm: **a** C0.5-1 sand; **b** C0.1-0.25 sand; **c** Q0.5-1 sand; **d** Q0.1-0.25 sand

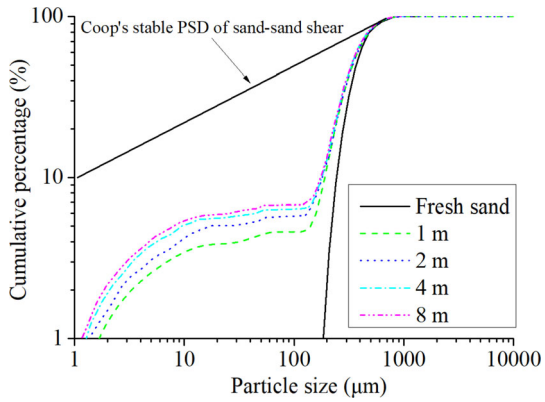

Fig. 19 Comparison of stable particle size distribution of interface shear and sand–sand shear in the case of large-displacement shear

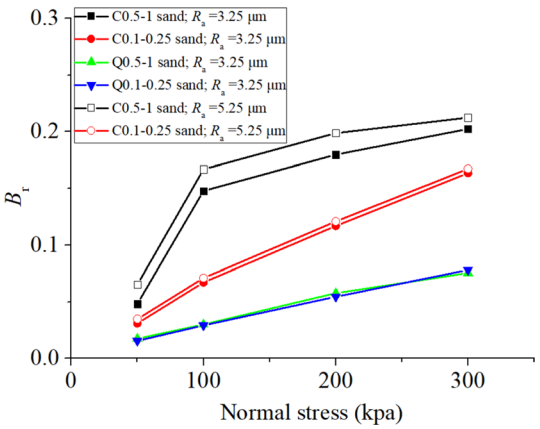

Fig. 20 Relationship between the relative breakage and normal stress at 2 m shear displacement

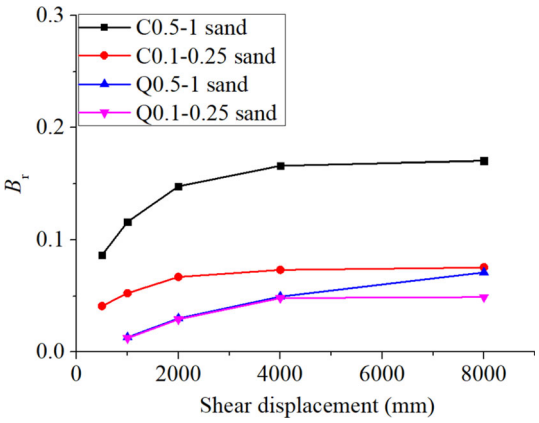

Fig. 21 Relationship between the relative breakage and shear displacement under normal stress of 100 kPa with R_a= 3.25 μm

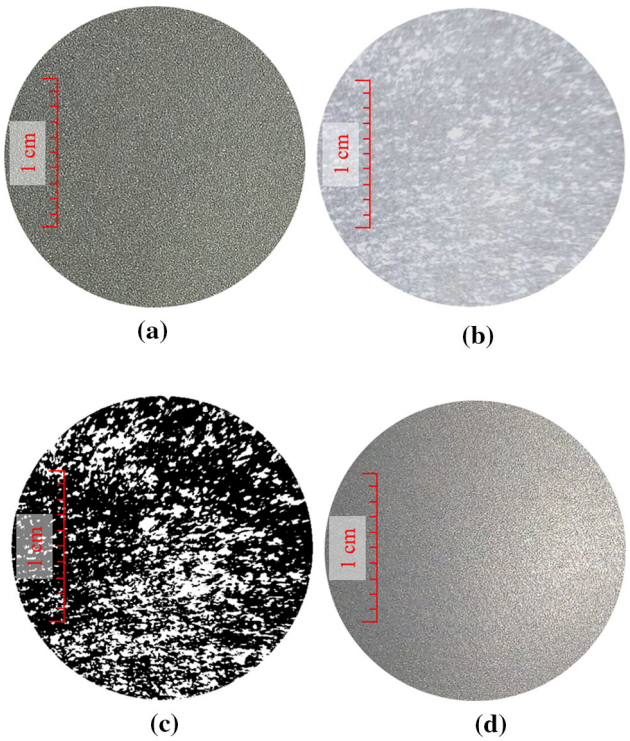

Fig. 22 Photos of the interface before and after experiments: **a** interface before test; **b** interface in M4(C0.5-1 sand under 300 kPa after 2 m displacement shear); **c** area occupation ratio of fine particle embedded interface **d** interface in M12 (Q0.5-1 sand under 300 kPa after 2 m displacement shear)

4 Discussions

4.1 Evolution of particle shape and particle size distribution

4.1.1 Particle shape

Figure 24 shows SEM photos of carbonate and quartz sand samples before and after interface shear. As shown in Fig. 24a, obvious pores and initial defects can be observed on the surface of fresh C0.5-1 sand. The original particles are irregular in shape and have many protuberances. After 2 m displacement shear, the particles become more slippery and rounded shown in Fig. 24b. And the rounded large particles are wrapped up with fine particles. Figure 24c, d presents SEM photographs of C0.1-0.25 sand. The fresh sand particles also have irregular sharp edges. After 2-m displacement interface shear, the shape of irregular particle become rounded, and there exists a lot of fine particles on the particle surface. Figure 24e, f gives the Q0.5-1 sand SEM photographs. Compared with C0.5-1 sand, the surfaces of quartz sand are relatively smooth. After 2 m displacement shear, the shape of large original particles remains almost unchanged, but fine particles formed from breakage are irregular. Figure 24g, h shows Q0.1-0.25 sand before and after interface shear. There is no significant change in the shape of large particles after interface shear.

Through the observation of a single particle movement by the transparent outer ring, it is concluded that the main movement of sand particles is the rolling between particles. During the interface shear process, fresh sand particles are broken and fine particles are constantly generated. However, because of the differences in mineral hardness, the shape evolution of carbonate sands and quartz sands show different behaviors. The grain hardness of the carbonate sands is relatively low. After the stress concentration in the protruding parts occurs, these parts gradually wear away, so the particles are more rounded and smoother. In contrast, the brittle fracture will occur for quartz sands due to its high hardness, so the shape of original particles can still be irregular.

4.1.2 Grain blank segment

The grain blank segment appears in PSD after the interface shear, e.g., the gradation is discontinuous, as shown in Figs. 16, 17 and 18. The explanation is as follows: When the protruding parts of large particles break up, the small particles from particle breakage are filled in the gap of large particles. With the increase in small particles, the gap between large particles is gradually filled, so the degree of

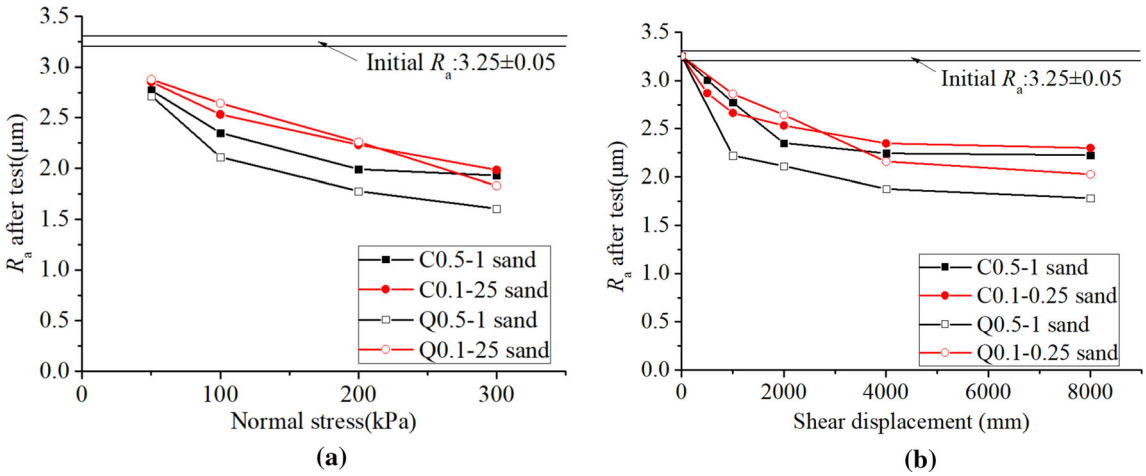

Fig. 23 Interface roughness: **a** against normal stress after 2 m displacement shear; **b** against shear displacement under 100 kPa

particle breakage gradually decreases until steady state is reached. Corresponding to the gradation curve, the upper boundary of the grain blank segment is the minimum size of large particles after breakage, and the lower boundary is the maximum size of new-formed fine particles formed from particle breakage.

The grain blank segment in PSD curve has a close relationship with mean particle size D_{50}. It is shown in Fig. 25a that the ratios of the upper and lower grain blank segment boundary sizes to the particle size D_{50} keep within a certain range, with about 0.35–0.43 for upper boundary and 0.15–0.21 for lower boundary. The grain blank segment mentioned above can also be seen in Fig. 25b. It shows the size range of the grain blank segment changes during the shear process. Specifically, the upper boundary ratio reduces with the increase in shear displacement and then tends to be stable, while the lower boundary ratio is basically stable with a small increase trend. It indicates that with the increase in displacement, the large particles continue to break to produce particles whose size does not exceed the lower boundary size.

4.2 Interface strength with shear displacement

Figure 26 shows the test results with R_a= 3.25 μm for a small displacement shear compared with DeJong's experiment result (2009). The interface shear between three kinds of sands (Glass beads with D_{50} = 0.95 mm, Ottawa 20–30 with D_{50} = 0.74 mm, Q-Rok with D_{50} = 0.75 mm) and intermediate surface (R_a = 6.2 μm) were conducted. DeJong's experiment result (2009) pointed out that except for the particle size and surface roughness, the particle shape also has effect on the shear behavior between sand and steel surface. The sands used in this paper show higher interface strength than the rounded Glass beads, but have lower strength compared to the subrounded Ottawa 20–30 sand and subangular Q-Rok. Another difference is that the displacement to mobilize the maximum shear stress. The tests in this paper need larger displacement (near 2–3 mm) to reach the stable strength, while DeJong's tests only need about 1 mm. The reason for the difference is thought to be the boundary condition difference between ring shear and direct interface shear.

The typical variation trends of the mobilized interface friction angle δ_{cs} with the increase in shear displacement are shown in Fig. 27. Except Q0.5-1 sand, the variations of δ_{cs} are similar and can be divided into four stages: The first stage corresponds to the state with uniform shear deformation of sand sample. At the end of this stage, the peak interface strength is fully mobilized. In the second stage, shear localization appears and the deformation band develops gradually with the particle rearrangement. Accordingly, the interface friction angle reduces. In the third stage, a large number of fine particles appear from obvious particle breakage. The fine particles are gradually filled into the gap between large particles, which makes the deformation band denser, thus increases the interface strength. At the last stage, the fine particles near the interface reach a certain dense state, and the interface strength tends to be stable. Exceptionally, the interface friction angle δ_{cs} for Q0.5-1 sand shows a continuous increase trend. This is mainly due to the increase in interaction area of Q0.5-1 sand with the interface during the whole interface shear process.

Figure 28 shows the relationship of normalized interface strength versus R_a/D_{50}. Dietz and Ling's experimental results [11] are also presented on the figure as comparisons (φ is the direct friction angle for sand–sand shear). It is found that the quartz sands' interface strength at 5 mm shear displacement coincides well with Dietz and Ling's experimental results [11]. However, when the shear displacement is large ($\geq$ 1 m), the interface strength is higher

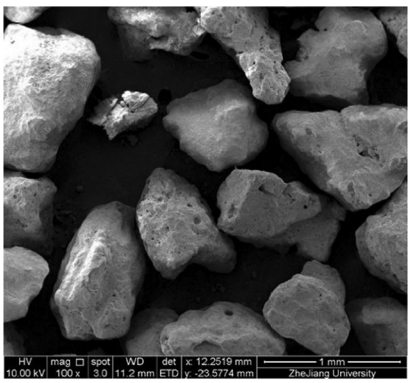
HV 10.00 kV | mag 100 x | spot 3.0 | WD 11.2 mm | det ETD | x: 12.2519 mm y: -23.5774 mm | 1 mm | ZheJiang University

(a)

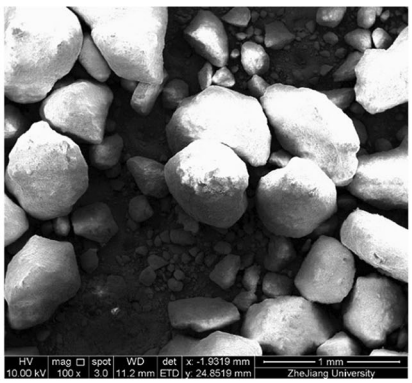
HV 10.00 kV | mag 100 x | spot 3.0 | WD 11.2 mm | det ETD | x: -1.9319 mm y: 24.8519 mm | 1 mm | ZheJiang University

(b)

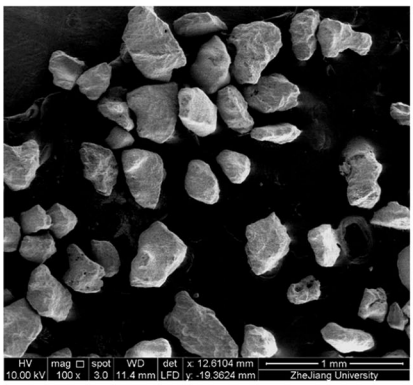
HV 10.00 kV | mag 100 x | spot 3.0 | WD 11.4 mm | det LFD | x: 12.6104 mm y: -19.3624 mm | 1 mm | ZheJiang University

(c)

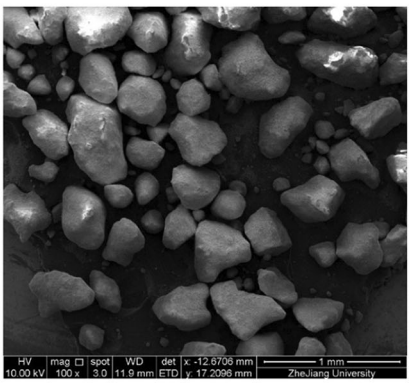
HV 10.00 kV | mag 100 x | spot 3.0 | WD 11.9 mm | det ETD | x: -12.6706 mm y: 17.2096 mm | 1 mm | ZheJiang University

(d)

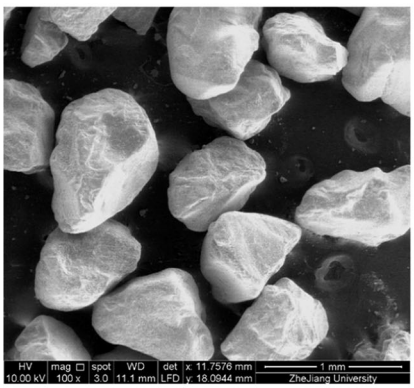
HV 10.00 kV | mag 100 x | spot 3.0 | WD 11.1 mm | det LFD | x: 11.7576 mm y: 18.0944 mm | 1 mm | ZheJiang University

(e)


HV 10.00 kV | mag 100 x | spot 3.0 | WD 11.3 mm | det LFD | x: -11.0189 mm y: 23.5669 mm | 1 mm | ZheJiang University

(f)

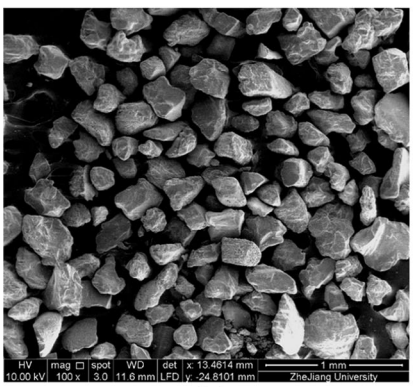
HV 10.00 kV | mag 100 x | spot 3.0 | WD 11.6 mm | det LFD | x: 13.4614 mm y: -24.8101 mm | 1 mm | ZheJiang University

(g)


HV 10.00 kV | mag 100 x | spot 3.0 | WD 11.0 mm | det LFD | x: 25.0874 mm y: -2.8091 mm | 1 mm | ZheJiang University

(h)

◀**Fig. 24** SEM photos of sands before and after interface shear under 100 kPa with R_a= 3.25 μm after 2 m displacement shear: **a** C0.5-1 sand before shear; **b** C0.5-1 sand after shear; **c** C0.1-0.25 sand before shear; **d** C0.1-0.25 sand after shear; **e** Q0.5-1 sand before shear; **f** Q0.5-1 sand after shear; **g** Q0.1-0.25 sand before shear; **h** Q0.1-0.25 sand after shear

than before, thus R_a/D_{50} is no longer suitable for assessing the interface friction angle. The main reason is that the fine particles are gradually filled into the gap between large particles, which makes the deformation band denser, thus increases the interface strength.

In order to consider the effect of fine particles on the interface strength, an impact factor β is defined according to the PSD before and after interface shear as follows:

$$\beta = \frac{S_r}{S} \tag{4}$$

where S_r is the approximate trapezoid area within the upper boundary of the platform section in Fig. 29(in red color), and S is rectangular area with the height of the fine content under the shear displacement of 8 m (shadow region).

The modified characteristic particle size D_m is defined as

$$D_m = (1 - \beta) * D_{50} \tag{5}$$

The relationship between δ_{cs}/φ and R_a/D_m is shown in Fig. 30. It is shown that the quartz sands' values of δ_{cs}/φ have a good linear relationship with the values of R_a/D_m, but carbonate sands have a higher interface strength over the fitting curve except the tests of 0.5 m shear displacement. Compared with the quartz sands, the carbonate sands have a large number of fine particles embedded in the interface during large-displacement shear(≥ 1 m), which makes parts of the shear interface convert to sand–sand shear of fine particles, thus increasing the interface

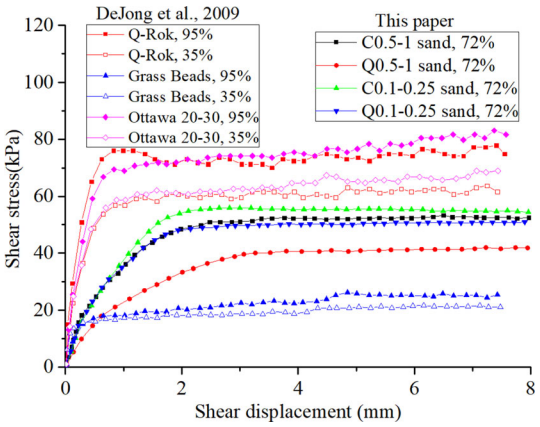

Fig. 26 Comparison with DeJong's experiment result (2009) under 100 kPa with R_a= 3.25 μm

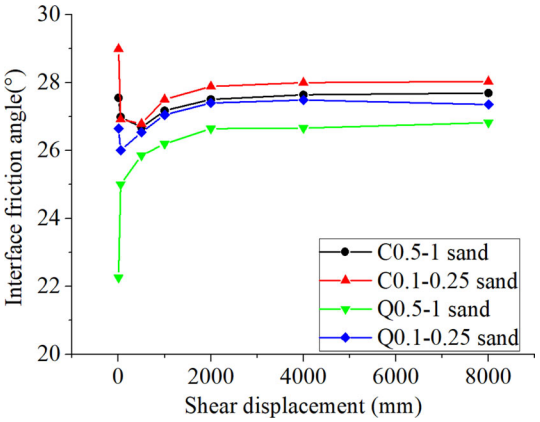

Fig. 27 Variations of δ_{cs} values along with the shear displacement

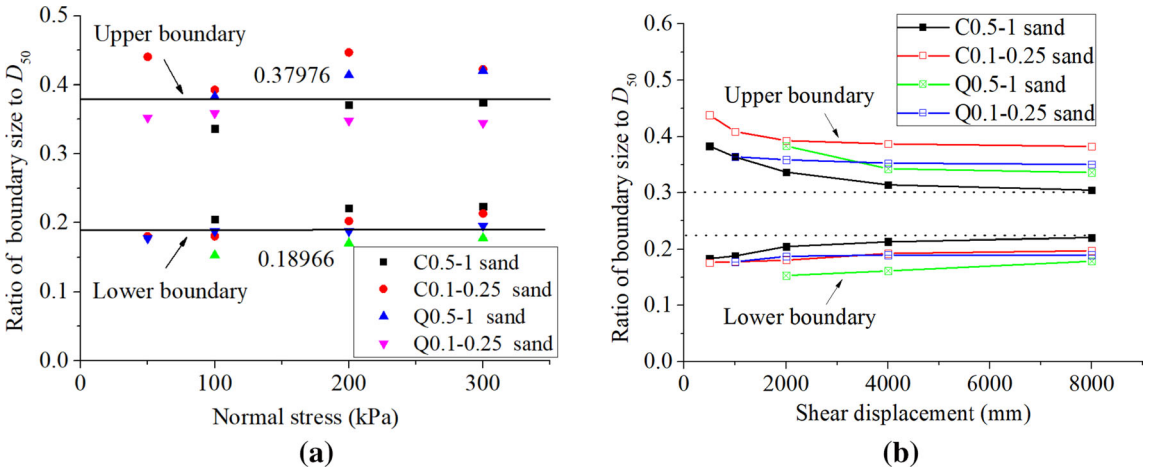

Fig. 25 The ratio of platform boundary to initial D_{50} with R_a= 3.25 μm: **a** versus normal stress; **b** versus shear displacement

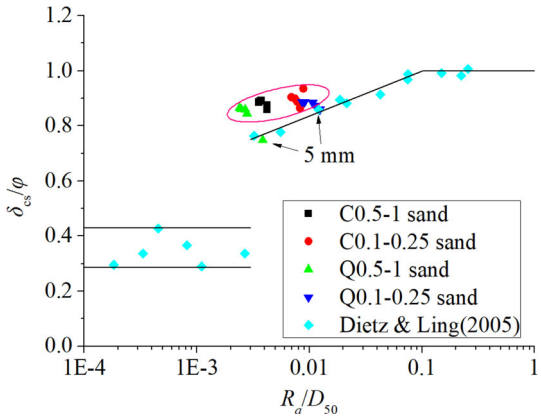

Fig. 28 Normalized interface strength versus R_a/D_{50}

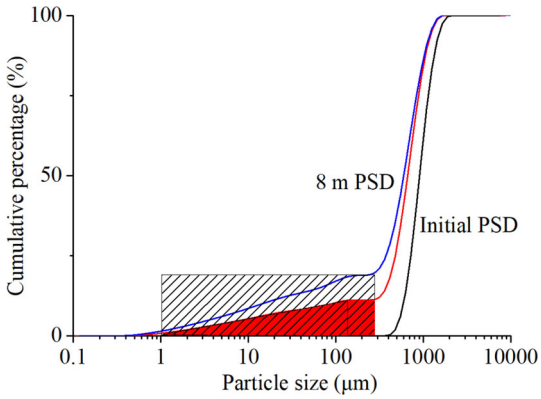

Fig. 29 A schematic diagram of the calculation method of β (color figure online)

strength. In particular, when no fine particles are produced, the β value is equal to 0 and the R_a/D_m value is degraded to the R_a/D_{50} value proposed by Dietz and Lings [11].

5 Conclusions

In this paper, a series of interface shear tests have been carried out to study the interface behavior between carbonate sand and steel. The effects of particle size, normal stress, and shear displacement on the interface shear strength were studied. Furthermore, the developments of deformation band and shear zone during interface shear were investigated, and the related physical mechanism was discussed. Through detailed studies, some main conclusions can be drawn as follows:

1. The interface friction angle between carbonate sand and steel is related to the shear displacement and normal stress. The interface friction angle always reaches a peak at the end of uniform deformation of sand sample, and then decreases after the shear localization. The interface friction angle will increase again with the increase in shear displacement due to a large amount of particle breakage, and finally stabilizes at a certain value. The increase in normal stress on the interface would lead to an obvious increase in interface strength for carbonate sands.
2. The development of deformation band has been investigated during the interface shear. It is found that the particles near the interface have obvious relative displacement with the interface. The thickness of shear zone is closely related to the particle size. It is about $5D_{50}$ for coarse sands and about $11D_{50}$ to $12D_{50}$ for fine sands. Increases of normal stress and shear displacement can make the particle breakage more severely, thus forming thicker and denser shear zone. Shear zone thickness keeps stable after the particles in the deformation band are fully broken.
3. There exists obvious discontinuity in the particle size distribution after large-displacement interface shear, i.e., a grain blank segment appears in PSD curve. The reason for this grain blank segment is that the shape and size of origin particles will be changed due to the damage of particle protruding parts. The minimum size of original particles after breakage is related to the upper boundary of the grain blank segment, and the maximum size of damaged protruding parts corresponds to the lower boundary.
4. The steel roughness has significant influence on the interface shear behavior. The relative smooth steel surface shows small interface friction angle without dilation phenomenon during shearing, while higher roughness leads to higher interface strength due to stress dilation. Higher deformation band thickness, bigger shear zone thickness, and apparent particle breakage appear under higher roughness condition,

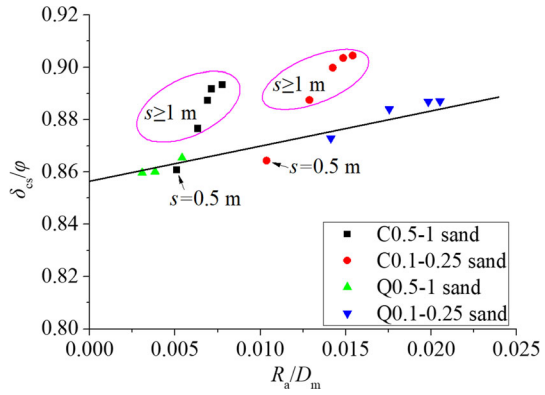

Fig. 30 The relationships between δ_{cs}/φ and R_a/D_m of different sand samples

indicating more intense interaction of sands and steel surface.

5. During the interface shear process, the average interface roughness R_a decreases with the increases of normal stress and shear displacement. Meanwhile, a large number of broken sand particles appear near the interface. Therefore, the original R_a/D_{50} is not appropriate for the assessment of interface strength in large-displacement interface shear. A modified R_a/D_m is proposed in this paper to consider the influence of interface roughness and particle breakage on the mobilization of interface strength between sands and steel. It is also noted that after large-displacement interface shear, the broken fine particles of carbonate sands are embedded in the steel interface and obviously increase the interface friction angle. It is recommended that the influence of embedded fine particles should be considered.

Acknowledgements The authors are grateful to the supports from the research project in the fields of High-tech Ships ([2016]22) of Ministry of Industry and Information Technology, National Natural Science Foundation of China (Grant Nos. 51779220 and 51209183), Zhejiang Provincial Natural Science Foundation of China (LY15E090002), Key Research and Development program of Zhejiang Province (2018C03031).

References

1. Alshibli KA, Sture S (2000) Shear band formation in plane strain experiments of sand. J Geotech Geoenviron Eng 126(6):495–503
2. ASTM (2017) A1040-17 standard guide for specifying harmonized standard grade compositions for wrought carbon, low-alloy, and alloy steels
3. Bishop A, Green G, Garga V, Anderson A, Brown J (1971) A new ring shear apparatus and its application of the measurement of the residual strength. Géotechnique 21(4):273–328.
4. Brandes HG (2011) Simple shear behavior of calcareous and quartz sands. Geotech Geol Eng 29(1):113–126
5. Coop MR, Sorensen KK, Freitas Bodas T, Georgoutsos G (2004) Particle breakage during shearing of a carbonate sand. Géotechnique 54(3):157–163
6. Datta M, Gulhati SK, Rao GV (1982) Engineering behavior of carbonate soils of India and some observations on classification of such soils. Geotech Prop Behav Perform Calcareous Soils 777:113–140
7. DeJong JT, Frost JD (2002) A multisleeve friction attachment for the cone penetrometer. Geotech Test J 25(2):111–127
8. DeJong JT, Westgate ZJ (2009) Role of initial state, material properties, and confinement condition on local and global soil-structure interface behavior. J Geotech Geoenviron Eng 135(11):1646–1660
9. DeJong JT, White DJ, Randolph MF (2003) Interface load transfer degradation during cyclic loading: a microscale investigation. Soils Found 43(4):81–93
10. DeJong JT, White DJ, Randolph MF (2006) Microstructure observation and modelling of soil-structure interface behavior using PIV. Soils Found 46(1):15–28
11. Dietz MS, Lings ML (2006) Post peak strength of interfaces in a stress–dilatancy framework. J Geotech Geoenviron Eng 132(11):1474–1484
12. Dove JE, Frost JD (1999) Peak friction behaviour of smooth geomembrane-particle interfaces. J Geotech Geoenviron Eng 125(7):544–555
13. Frost JD, Hebeler GL, Evans TM, DeJong JT (2004) Interface behaviour of granular soils. In: Proceedings of earth and space conference, Houston, TX, pp 65–72
14. Hardin BO (1985) Crushing of soil particles. J Geotech Eng 111(10):1177–1192
15. Ho TYK, Jardine RJ, Anh-Minh N (2011) Large-displacement interface shear between steel and granular media. Géotechnique 61(3):221–234
16. Hyodo M, Aramaki N, Itoh M, Hyde AFL (1996) Cyclic strength and deformation of crushable carbonate sand. Soil Dyn Earthq Eng 15(5):331–336
17. Hyodo M, Hyde AFL, Aramaki N (1998) Liquefaction of crushable soils. Géotechnique 48(4):527–543
18. Jardine RJ, Lehane BM, Everton SJ (1992) Friction coefficients for piles in sands and silts. In: Proceeding 4th international conference on offshore site investigation and foundation behaviour, London, pp 661–677
19. Kwag JM, Ochiai H, Yasufuku N (1999) Yielding stress characteristics of carbonate sand in relation to individual particle fragmentation strength. In: Proceeding of international conference on engineering for calcareous sediments, the Netherlands, pp 79–87
20. Lings ML, Dietz MS (2005) The peak strength of sand-steel interfaces and the role of dilation. Soils Found 45(6):1–14
21. Miao G, Airey D (2013) Breakage and ultimate states for a carbonate sand. Géotechnique 63(14):1221–1229
22. Mortara G, Ghionna M, Ghionna VN (2007) Cyclic shear stress degration and post-cyclic behavior from sand-steel interface direct shear tests. Can Geotech J 44(7):739–752
23. Paikowsky SG, Player CM, Connors PJ (1995) A dual interface apparatus for testing unrestricted friction of soil along solid surfaces. Geotech Test J 18(2):168–193
24. Potyondy JG (1961) Skin friction between various soils and construction materials. Geotechnique 11(4):339–353
25. Rao KSS, Allam MM, Robinson RG (1998) Interfacial friction between sands and solid surfaces. Geotech Eng 131(2):75–82
26. Roscoe KH (1970) Tenth Rankine lecture: the influence of strains in soil mechanics. Géotechnique 20(2):129–170
27. Sadrekarimi AS, Olson SMOM (2010) Particle damage observed in ring shear tests on sands. Can Geotech J 47(5):497–515
28. Sadrekarimi A, Olson SM (2009) A new ring shear device to measure the large displacement shearing behavior of sands. Geotech Test J 32(3):197–208
29. Sadrekarimi A, Olson SM (2010) Shear band formation observed in ring shear tests on sandy soils. J Geotech Geoenviron Eng 136(2):366–375
30. Salem M, Elmamlouk H, Agaiby S (2013) Static and cyclic behavior of North Coast calcareous sand in Egypt. Soil Dyn Earthq Eng 55:83–91
31. Sharma SS, Ismail MA (2006) Monotonic and cyclic behavior of two calcareous soils of different origins. J Geotech Geoenviron Eng 132(12):1581–1591

32. Torabi A, Braathen A, Cuisiat F, Fossen H (2007) Shear zones in porous sand: insights from ring-shear experiments and naturally deformed sandstones. Tectonophysics 437:37–50
33. Wei HZ, Zhao T, He JQ, Meng QS, Wang XZ (2018) Evolution of particle breakage for calcareous sands during ring shear tests. Int J Geomech 18(2):04017153
34. Yang ZX, Jardine RJ, Zhu BT, Foray P, Tsuha CHC (2010) Sand grain crushing and interface shearing during displacement pile installation in sand. Geotechnique 60(6):469–482
35. Zhang X, Hu W, Scaring G, Baudet BA, Han W (2018) Particle shape factors and fractal dimension after large shear strains in carbonate sand. Géotech Lett 8:73–79

Publisher's Note Springer Nature remains neutral with regard to jurisdictional claims in published maps and institutional affiliations.